Compact and portable open-path sensor for simultaneous measurements of atmospheric N_2O and CO using a quantum cascade laser

Lei Tao,[1,2] Kang Sun,[1,2] M. Amir Khan,[1,2] David J. Miller,[1,2] and Mark A. Zondlo[1,2,*]

[1]*Department of Civil and Environmental Engineering, Princeton University, Princeton, New Jersey 08544, USA*
[2]*Center for Mid-Infrared Technologies for Health and the Environment, Princeton, New Jersey 08544, USA*
[*]*mzondlo@princeton.edu*

Abstract: A compact and portable open-path sensor for simultaneous detection of atmospheric N_2O and CO has been developed with a 4.5 μm quantum cascade laser (QCL). An in-line acetylene (C_2H_2) gas reference cell allows for continuous monitoring of the sensor drift and calibration in rapidly changing field environments and thereby allows for open-path detection at high precision and stability. Wavelength modulation spectroscopy (WMS) is used to detect simultaneously both the second and fourth harmonic absorption spectra with an optimized dual modulation amplitude scheme. Multi-harmonic spectra containing atmospheric N_2O, CO, and the reference C_2H_2 signals are fit in real-time (10 Hz) by combining a software-based lock-in amplifier with a computationally fast numerical model for WMS. The sensor consumes ~50 W of power and has a mass of ~15 kg. Precision of 0.15 ppbv N_2O and 0.36 ppbv CO at 10 Hz under laboratory conditions was demonstrated. The sensor has been deployed for extended periods in the field. Simultaneous N_2O and CO measurements distinguished between natural and fossil fuel combustion sources of N_2O, an important greenhouse gas with poorly quantified emissions in space and time.

©2012 Optical Society of America

OCIS codes: (280.3420) Laser sensors; (010.1120) Air pollution monitoring; (300.6340) Spectroscopy, infrared; (120.4640) Optical instruments.

References and links

1. Intergovernmental Panel on Climate Change, "Climate Change 2007: Synthesis Report," Core Writing Team, Pachauri, R.K. and Reisinger, A, eds. (Geneva, SwitzerLand, 2008)
2. S. A. Montzka, E. J. Dlugokencky, and J. H. Butler, "Non-CO_2 greenhouse gases and climate change," Nature **476**(7358), 43–50 (2011).
3. A. R. Ravishankara, J. S. Daniel, and R. W. Portmann, "Nitrous oxide N_2O: the dominant ozone-depleting substance emitted in the 21st century," Science **326**(5949), 123–125 (2009).
4. L. Joly, T. Decarpenterie, N. Dumelie, X. Thomas, I. Mappe-Fogaing, D. Mammez, R. Vallon, G. Durry, B. Parvitte, M. Carras, X. Marcadet, and V. Zeninari, "Development of a versatile atmospheric N2O sensor based on quantum cascade laser technology at 4.5 μm," Appl. Phys. B: Lasers Opt. **103**(3), 717–723 (2011).
5. A. Neftel, C. Flechard, C. Ammann, F. Conen, L. Emmenegger, and K. Zeyer, "Experimental assessment of N_2O background fluxes in grassland systems," Tellus B Chem. Phys. Meterol. **59**(3), 470–482 (2007).
6. R. Provencal, M. Gupta, T. G. Owano, D. S. Baer, K. N. Ricci, A. O'Keefe, and J. R. Podolske, "Cavity-enhanced quantum-cascade laser-based instrument for carbon monoxide measurements," Appl. Opt. **44**(31), 6712–6717 (2005).
7. A. D. Farinas, D. Balslev-Clausen, and E. Crosson, "A Mid-IR, wavelength-scanned, cavity ring-down spectrometer for continuous trace N_2O and nitrogen isotope measurements," abstract #B53C–0409, in *American Geophysical Union, Fall Meeting* (San Francisco, 2009).
8. J. P. Lima, H. Vargas, A. Miklos, M. Angelmahr, and P. Hess, "Photoacoustic detection of NO_2 and N_2O using quantum cascade lasers," Appl. Phys. B: Lasers Opt. **85**(2-3), 279–284 (2006).
9. S. Borri, S. Bartalini, P. De Natale, M. Inguscio, C. Gmachl, F. Capasso, D. L. Sivco, and A. Y. Cho, "Frequency modulation spectroscopy by means of quantum-cascade lasers," Appl. Phys. B: Lasers Opt. **85**(2-3), 223–229 (2006).

#177525 - $15.00 USD Received 5 Oct 2012; revised 21 Nov 2012; accepted 21 Nov 2012; published 3 Dec 2012
(C) 2012 OSA

10. C. Guimbaud, V. Catoire, S. Gogo, C. Robert, M. Chartier, F. Laggoun-Defarge, A. Grossel, P. Alberic, L. Pomathiod, B. Nicoullaud, and G. Richard, "A portable infrared laser spectrometer for flux measurements of trace gases at the geosphere-atmosphere interface," Meas. Sci. Technol. **22**(7), 075601 (2011).
11. D. McDermitt, G. Burba, L. Xu, T. Anderson, A. Komissarov, B. Riensche, J. Schedlbauer, G. Starr, D. Zona, W. Oechel, S. Oberbauer, and S. Hastings, "A new low-power, open-path instrument for measuring methane flux by eddy covariance," Appl. Phys. B: Lasers Opt. **102**(2), 391–405 (2011).
12. J. Chen, A. Hangauer, R. Strzoda, and M. C. Amann, "VCSEL-based calibration-free carbon monoxide sensor at 2.3 μm with in-line reference cell," Appl. Phys. B: Lasers Opt. **102**(2), 381–389 (2011).
13. K. Sun, L. Tao, D. J. Miller, M. A. Khan, and M. A. Zondlo, "Inline Multi-harmonic Calibration Method for Open-path Atmospheric Ammonia Measurements," Appl. Phys. B-Lasers O. doi:10.1007/s00340-012-5231-2 (2012).
14. P. Kluczynski and O. Axner, "Theoretical description based on Fourier analysis of wavelength-modulation spectrometry in terms of analytical and background signals," Appl. Opt. **38**(27), 5803–5815 (1999).
15. P. Kluczynski, A. M. Lindberg, and O. Axner, "Background signals in wavelength-modulation spectrometry with frequency-doubled diode-laser light. I. Theory," Appl. Opt. **40**(6), 783–793 (2001).
16. M. A. Zondlo, M. E. Paige, S. M. Massick, and J. A. Silver, "Vertical cavity laser hygrometer for the National Science Foundation Gulfstream-V aircraft," J. Geophys. Res., [Atmos.] **115**(D20), D20309 (2010).
17. S. Schilt, L. Thévenaz, and P. Robert, "Wavelength modulation spectroscopy: combined frequency and intensity laser modulation," Appl. Opt. **42**(33), 6728–6738 (2003).
18. H. J. Li, G. B. Rieker, X. Liu, J. B. Jeffries, and R. K. Hanson, "Extension of wavelength-modulation spectroscopy to large modulation depth for diode laser absorption measurements in high-pressure gases," Appl. Opt. **45**(5), 1052–1061 (2006).
19. J. Reid and D. Labrie, "Second-harmonic detection with tunable diode lasers—comparison of experiment and theory," Appl. Phys. B: Lasers Opt. **26**(3), 203–210 (1981).
20. S. Schilt and L. Thévenaz, "Experimental method based on wavelength-modulation spectroscopy for the characterization of semiconductor lasers under direct modulation," Appl. Opt. **43**(22), 4446–4453 (2004).
21. A. Neftel, C. Ammann, C. Fischer, C. Spirig, F. Conen, L. Emmenegger, B. Tuzson, and S. Wahlen, "N_2O exchange over managed grassland: Application of a quantum cascade laser spectrometer for micrometeorological flux measurements," Agric. For. Meteorol. **150**(6), 775–785 (2010).
22. L. S. Rothman, I. E. Gordon, A. Barbe, D. C. Benner, P. F. Bernath, M. Birk, V. Boudon, L. R. Brown, A. Campargue, J.-P. Champion, K. Chance, L. H. Coudert, V. Dana, V. M. Devi, S. Fally, J.-M. Flaud, R. R. Gamache, A. Goldman, D. Jacquemart, I. Kleiner, N. Lacome, W. Lafferty, J.-Y. Mandin, S. T. Massie, S. N. Mikhailenko, C. E. Miller, N. Moazzen-Ahmadi, O. V. Naumenko, A. V. Nikitin, J. Orphal, V. I. Perevalov, A. Perrin, A. Predoi-Cross, C. P. Rinsland, M. Rotger, M. Simeckova, M. A. H. Smith, K. Sung, S. A. Tashkun, J. Tennyson, R. A. Toth, A. C. Vandaele, and J. Vander Auwera, "The *HITRAN* 2008 molecular spectroscopic database," J. Quant. Spectrosc. Radiat. Transf. **110**(9-10), 533–572 (2009).
23. L. Tao, K. Sun, D. J. Miller, M. A. Khan, and M. A. Zondlo, "Current and frequency modulation characteristics for continuous-wave quantum cascade lasers at 9.06 μm," Opt. Lett. **37**(8), 1358–1360 (2012).
24. J. A. Silver, "Simple Dense-pattern Optical Multipass Cells," Appl. Opt. **44**(31), 6545–6556 (2005).
25. J. B. McManus, P. L. Kebabian, and M. S. Zahniser, "Astigmatic mirror multipass absorption cells for long-path-length spectroscopy," Appl. Opt. **34**(18), 3336–3348 (1995).
26. R. A. Whitby and E. R. Altwicker, "Acetylene in the atmosphere: Sources, representative ambient concentrations and ratios to other hydrocarbons," Atmos. Environ. **12**(6-7), 1289–1296 (1978).
27. A. Hangauer, J. Chen, R. Strzoda, and M.-C. Amann, "Multi-harmonic detection in wavelength modulation spectroscopy systems," Appl. Phys. B-Lasers O. doi:10.1007/s00340-012-5049-y (2012).
28. G. B. Rieker, J. B. Jeffries, and R. K. Hanson, "Calibration-free wavelength-modulation spectroscopy for measurements of gas temperature and concentration in harsh environments," Appl. Opt. **48**(29), 5546–5560 (2009).
29. P. Werle, R. Mücke, and F. Slemr, "The limits of signal averaging in atmospheric trace-gas monitoring by tunable diode-laser absorption spectroscopy (TDLAS)," Appl. Phys. B: Lasers Opt. **57**, 131–139 (1993).
30. D. Zona, I. A. Janssens, M. S. Verlinden, L. S. Broeckx, J. Cools, B. Gioli, A. Zaldei, and R. Ceulemans, "Impact of extreme precipitation and water table change on N_2O fluxes in a bio-energy poplar plantation," Biogeosciences Discuss. **8**(2), 2057–2092 (2011).
31. J. Dick, U. Skiba, and J. Wilson, "The effect of rainfall on NO and N_2O emissions from Ugandan agroforest soils," Phyton (Austria) **41**, 73–80 (2001).
32. US EPA, "Emission Facts: Average Annual Emissions and Fuel Consumption for Passenger Cars and Light Trucks," Office of Transportation and Air Quality, ed. (2000).
33. US EPA, "Update of Methane and Nitrous Oxide Emission Factors for On-Highway Vehicles," Office of Transportation and Air Quality, ed. (2004).
34. D. E. Burch, E. B. Singleton, and D. Williams, "Absorption line broadening in the infrared," Appl. Opt. **1**(3), 359–363 (1962).

#177525 - $15.00 USD Received 5 Oct 2012; revised 21 Nov 2012; accepted 21 Nov 2012; published 3 Dec 2012
(C) 2012 OSA

1. Introduction

Nitrous oxide (N_2O) is the third most important anthropogenic greenhouse gas with a global warming potential ~300 times that of carbon dioxide (CO_2) on a per molecule basis and a long lifetime of ~120 years [1,2]. Its concentration is rapidly increasing in the atmosphere (currently ~325 ppbv, ~0.7 ppbv yr^{-1}), but its emissions are poorly constrained in space and time, despite its importance to global climate change and ozone depletion [3]. There is an urgent need for instruments that can identify and resolve the spatial and temporal variances in N_2O emissions, particularly in field environments where power and shelter are not readily available. Indeed, no sensors for N_2O exist that can be portable and easily deployed yet still meet the measurement specifications of high-precision (~1 ppbv) and stability.

Taking advantage of the fundamental absorption bands in the mid-infrared, many quantum cascade laser (QCL)-based N_2O sensors have been developed with different spectroscopy methods such as TDLS (Tunable Diode Laser Spectroscopy) [4,5], ICOS (Integrated Cavity Output Spectroscopy) [6], CRDS (Cavity Ring-Down Spectroscopy) [7], PAS (Photoacoustic Spectroscopy) [8] and FMS (Frequency Modulation Spectroscopy) [9]. However, most available sensors are closed-path systems with high sample gas flows at significantly reduced optical cell pressures in order to achieve fast response times (i.e. 10 Hz) and spectrally isolated absorption features. Due to the requirement of a vacuum pump, these sensor systems consume hundreds to thousands Watts of power and have masses in excess of 100 kg [4,10]. This severely restricts practical applicability for continuous monitoring in remote or portable field studies and limits spatial coverage of measurements [11]. Besides, a closed-path sensor is not a non-intrusive detection scheme with the sample gas flowing through tubes, filter and chamber, which introduces sampling artifacts such as time lags, pressure regulation, and broadening of high-frequency changes in atmospheric structure.

We describe a new approach for open-path detection for atmospheric N_2O that allows for compact and portable sensors yet maintains the necessary high-precision and stability. A continuous, in-line reference absorption signal is used to address instrument drift in rapidly-changing environmental conditions, and multi-harmonic wavelength modulation spectroscopy is used to isolate complex, overlapping spectral absorption features typical of ambient pressures. Our sensor addresses the challenges of maintaining high-precision and stability for open-path N_2O measurements through two approaches. First, the continuous in-line reference cell uses a different gas within the laser scan range to address sensor drift resulting from high-frequency changes in the environment. While Chen *et al.* [12] and Sun *et al.* [13] have also used this approach, the former study was in a controlled laboratory environment while the latter study had more relaxed measurement requirements (~10% accuracy) that are insufficient for atmospheric N_2O. Second, digital wavelength modulation spectroscopy (WMS) detection is used to simultaneously detect and numerically fit multiple harmonic spectra at high-frequency and precision with a new numerical model.

In addition to N_2O, our sensor also simultaneously detects carbon monoxide (CO) and thereby provides additional insight on the various sources for N_2O emissions. Even though the major sources of atmospheric N_2O are biogenic processes (nitrification and denitrification) in soils and aquatic systems [1], anthropogenic activities (e.g. industrial nitrogen fixation, agriculture and the burning of fossil fuels) perturb the nitrogen cycle and thus account for the recent increase of atmospheric N_2O concentrations [2]. CO is an important tracer for anthropogenic activities related to combustion such as the burning of fossil fuels. Simultaneous detection of these two gases helps to identify whether N_2O sources are of biogenic or anthropogenic origin and consequently yields a better understanding on the influence of anthropogenic activities (e.g. combustion) on global climate change.

Our sensor uses a thermoelectrically-cooled, continuous wave, distributed feedback 4.54 μm QCL and has a mass of ~15 kg, electrical power consumption of ~50 W, and size of 50 x 18 x15 cm. The sensor measures at 10 Hz with a precision of 0.15 ppbv N_2O and 0.36 ppbv

#177525 - $15.00 USD Received 5 Oct 2012; revised 21 Nov 2012; accepted 21 Nov 2012; published 3 Dec 2012
(C) 2012 OSA

CO, simultaneously. It is the first demonstration of a compact, open-path QCL-based sensor for N_2O, to our knowledge. The low power consumption, compact size, portable nature, and calibration-maintaining design makes the sensor easy to be deployed in the field with robust performance. Open-path detection of N_2O has never been achieved at the requisite precision and stability and provides a pathway for compact, portable, stable, and low power sensors for understanding N_2O fluxes to the atmosphere.

2. Spectroscopic methodology and laser characterizations

2.1 Numerical model for wavelength-modulation spectroscopy signals

WMS is a widely applied technique for sensitive measurements of trace gas species [14,15]. The basic method involves a similar idea to direct-absorption spectroscopy, with an additional fast sinusoid (at frequency *f*) modulation applied to the laser current (wavelength). The modulated absorption signal on the photo-detector is then processed though a lock-in amplifier which demodulates the signal at the fundamental modulation frequency and its integral multiples (harmonics) – also known as synchronous phase sensitive detection. In other words, WMS increases sensitivity by shifting to a higher frequency detection bandwidth and rejecting noise (e.g. *1/f* laser noise) with lock-in amplifiers. WMS is particularly useful for probing air-broadened and overlapping absorption features in open-path sensors [16].

Instead of using analytic derivations of WMS from the Fourier series [17–19], we instead develop a model based upon numerical simulation of lock-in amplifier output signals. In WMS, both the laser current $i(t)$ and laser frequency $\nu(t)$ are the superposition of a high frequency sinusoidal modulation (f_m) with a low frequency sawtooth scan (f_s). For one sawtooth period ($0 \le t \le 1/f_s$), the equations take the form:

$$i(t) = i_0 + i_s \cdot f_s \cdot t + i_m \cdot \cos(2\pi f_m t) \tag{1}$$

$$\nu(t) = \nu_0 + \eta(f_s) \cdot i_s f_s t + \eta(f_m) \cdot i_m \cdot \cos[2\pi f_m t + \phi(f_m)] \tag{2}$$

where i_0 and ν_0 are the baseline of input current to the laser and its frequency, respectively. Two frequency-dependent functions are the laser frequency tuning rate ($\eta(f)$, GHz/mA) and the phase shift ($\phi(f)$, radians) between current amplitude and frequency modulation. Both $\eta(f)$ and $\phi(f)$ need to be characterized for the specific laser used [17, 18, 20]. The intensity of the laser $I(t)$ as well as the detector signal $D(t)$ for multiple absorption lines can be derived with Eq. (1) and Eq. (2) as following:

$$I(t) = A_0 + A_1 i(t) + A_2 i(t)^2 + A_3 i(t)^3 \tag{3}$$

$$D(t) = \chi \cdot I(t) \cdot \exp[-\sum_i x_i S_i L_i \psi_i(T, P, \nu(t))] \tag{4}$$

Variable A_i (presented up to the third order) in Eq. (3) can be easily retrieved by fitting laser current and intensity curve with a polynomial function. In the detector signal $D(t)$, χ is a collection efficiency factor of the detector, which includes the loss from reflection, scattering and detector geometry efficiency. x_i, S_i and L_i in Eq. (4) are the number density, the absorption line strength and the path-length for different absorption lines, respectively. $\psi_i(T, P, \nu(t))$ is the frequency dependant line-shape function, which also depends on the temperature T and pressure P, and can be modeled with a Doppler (Gaussian), Lorentzian or Voigt profile. The detector signal, $D(t)$, is multiplied to a reference signal $R(t)$ given by:

$$R(t) = \sin(n \cdot f_m \cdot 2\pi t + \varphi) \tag{5}$$

where n is the order of the harmonic and φ is the phase difference between the reference and the modulated detector signal. In our numerical model, the underlying assumption for all time

#177525 - $15.00 USD Received 5 Oct 2012; revised 21 Nov 2012; accepted 21 Nov 2012; published 3 Dec 2012
(C) 2012 OSA

varying signals satisfies the Nyquist sampling theorem, i.e. a constant time spacing of Δt with $1/\Delta t > 2f_m$. The product of the time series $D(t)R(t)$ signal is input to a 4th order low pass infinite impulse response (IIR) Butterworth filter to obtain the DC component equivalent to the n^{th} harmonic of the input signal. We use this model to simulate and perform fittings to different harmonics. The 2f (n = 2) signal is the most widely used harmonic in WMS due to its high SNR and peak of the signal at the line center for easy interpretation. The magnitude of the n^{th} harmonic is also dependent on modulation index m defined as

$$m = \frac{\nu_m}{\Delta\nu} = \frac{\eta(f_m)i_m}{\Delta\nu} \tag{6}$$

where $\Delta\nu$ is the half width at half maximum (HWHM) of the absorption line, and ν_m is the laser frequency modulation amplitude. The well-studied relationship between the 2f signal and the modulation index m is used to validate the numerical model. Figure 1 shows the comparison between our numerical model and the analytical model based on Li *et al.* [18] to study the 2f signal height as a function of modulation index m with different line shape functions. The maximum 2f peak height can be achieved with a modulation index of m ~2.2 with both Doppler and Lorentzian line-shape functions. There is an excellent agreement on the results from two models with residuals less than 0.1%, which is due to the leakage of the spectral components for discrete signals used in the numerical model. A high sample rate (a small Δt) can help to minimize this residual. Compared to the analytical model, our new numerical model runs much faster with a computationally simpler approach, which naturally combines the laser intensity and frequency modulation [17]. The new numerical model for WMS provides a powerful tool for comparison between experimental results and simulations with the capability of performing spectral fitting for multi-harmonic signals.

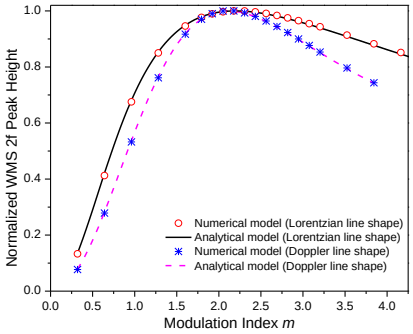

Fig. 1. Comparison between analytical and numerical models.

2.2 Characterization of QCL for WMS

N_2O has its fundamental vibrational band with the N-N stretch mode (Σ^+, ν_3) around 4.5 μm. Multiple QCL-based N_2O sensors [4,10,21] have already been reported around this wavelength. A Hamamatsu continuous wave (CW) TE-cooled DFB QCL operating at a wavelength at 4.52-4.54 μm was the light source for simultaneous detection of N_2O and CO. The laser output from the QCL was first tested and characterized with a wavemeter (Bristol 721 spectrum analyzer) to obtain laser wavelength and temperature curves. Figure 2 shows the characterization of the QCL's tuning range and the simulated detectable absorption lines. The QCL's output frequency is nearly linearly proportional to the applied current at a certain temperature. The simulated absorption lines were calculated from the HITRAN database for a 1 cm path length at room temperature, atmospheric pressure, and typical atmospheric concentrations of other relevant gases that absorb within this region [22]. Also plotted in Fig. 2 are the absorption lines of acetylene (C_2H_2) which are used as a reference gas for calibration

#177525 - $15.00 USD Received 5 Oct 2012; revised 21 Nov 2012; accepted 21 Nov 2012; published 3 Dec 2012
(C) 2012 OSA

of the N_2O (P(23) line) and CO within a single laser scan using WMS. For simultaneous detection of N_2O and CO, there is one spectral region of interest in our possible wavelength scan range: the P(22) to P(23) N_2O lines, which includes an overlapping CO line between two N_2O lines. This region also has little influence from nearby water vapor absorption lines. Therefore, the region between P(22) and P(23) N_2O lines was chosen for simultaneous detection of N_2O and CO with the laser operated at ~40°C. The detailed usage of the C_2H_2 reference is discussed below.

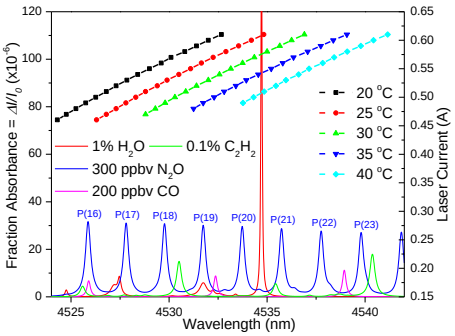

Fig. 2. Characterization of QCL tuning range on top of the detectable absorption lines.

Besides checking the tuning range of the QCL, it is very important to characterize functions of $\eta(f)$ and $\phi(f)$ as discussed above. A simple experiment was conducted to derive the frequency dependant tuning rate and phase shift of the QCLs as described in Tao *et al.* [23]. The frequency tuning rate measurements of this QCL were only conducted with 20 kHz modulation frequency and 20 mA modulation current amplitude. The tuning rate of the laser is 0.013 cm^{-1}/mA and 0.015 cm^{-1}/mA for operation temperature at 25°C and 40°C, respectively. The phase shift for both conditions is around 1.12π radian.

3. Experimental

3.1 Sensor setup

The schematic of the sensor setup is shown in Fig. 3. The TE-cooled Hamamatsu QCL in a high heat load (HHL) package was used as the monochromatic light source. The QCL was thermally controlled with a precise temperature controller (Wavelength Electronics, HTC3000) and driven by a low noise power supply (Wavelength Electronics, QCL1000). The laser beam traversed through a 5-cm long C_2H_2 reference cell (Wavelength References) after first being collimated by an AR-coated ZnSe lens and then was directed into a multi-pass optical cell with two mirrors. The reference cell had wedged and angled BaF_2 windows to suppress back reflections and was filled with 100 Torr pure C_2H_2 gas (at 20°C). The multi-pass cell consisted of two cylindrical mirrors (f = 250 mm, diameter 50.8 mm) using the methods described by Silver 2005 [24]. Cylindrical mirrors are relatively inexpensive and adaptable compared to highly precise astigmatic mirrors, which are commonly used to build long path length multi-pass cells [25]. By adjusting the distance and relative angle of the axis between two cylindrical mirrors, dense spot patterns as shown in Fig. 3 can be readily achieved. Our 15-cm long compact multi-pass cell was built with cage mounts and provided a 16 m long optical path length. The output laser beam was focused onto a thermoelectrically-cooled mercury cadmium telluride (MCT, Hamamatsu P2750) detector. The signal from MCT detector was first amplified with a current pre-amplifier (Hamamatsu C5185) and further processed by a USB multifunction data acquisition (DAQ) module (National Instruments, USB-6251). The sensor head is compact with a dimension of 50 x 18 x 15 cm as shown in Fig. 4. The electronics for the laser temperature and current control were integrated into one single instrument box.

#177525 - $15.00 USD Received 5 Oct 2012; revised 21 Nov 2012; accepted 21 Nov 2012; published 3 Dec 2012
(C) 2012 OSA

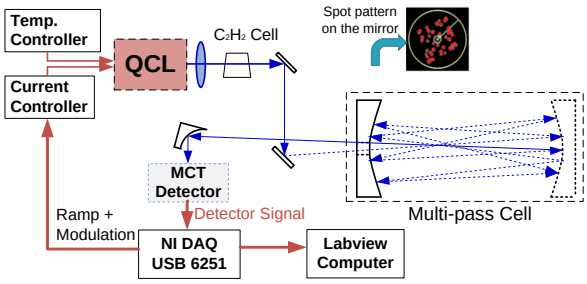

Fig. 3. Schematic of the sensor setup.

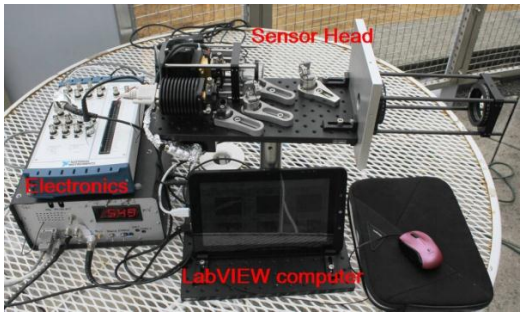

Fig. 4. Photo of the N_2O/CO sensor.

Instead of using a standalone hardware lock-in amplifier, a LabVIEW-based software lock-in amplifier identical to the numerical model described above was created to perform multi-harmonic detection. The custom LabVIEW program controlled the DAQ to simultaneously generate an analog signal and digitize the MCT detector signal at a sample rate of 1 MHz. The generated analog signal, which was a superposition of a slow frequency ramp (100 Hz) and a fast frequency sinusoidal modulation (20 kHz), was input to the laser current driver to scan and modulate the laser frequency. On the other end, the detector signal was digitized into the computer. The two processes were synchronized by triggering with the same internal counter of the DAQ. After performing the initial signal average (e.g. to 10 Hz), the detector signal was then processed though a simulated lock-in amplifier using a 4th order low-pass IIR Butterworth filter in LabVIEW. Multiple harmonics of the detector signal were calculated simultaneously, e.g. 1f, 2f and 4f or higher. At the same time, an active feedback control loop was applied in the software to lock the relative position of the line center (or even harmonics center peak) by adjusting the offset voltage of the analog output signal. The entire N_2O/CO sensor consumed ~50 W with a mass of ~15 kg. About half of the power consumption was from the laptop computer, which controls the LabVIEW program.

3.2 Optimization for simultaneous detection

The air-broadened linewidths of N_2O and CO have significantly different values. In HITRAN database [22], the HWHM for CO (~0.053 cm^{-1}/atm) is about ~70% of that for N_2O (~0.074 cm^{-1}/atm) for the targeted spectral lines. As discussed above, a modulation index of m ~2.2 yields the maximum amplitude of the 2f signal and thus the largest the SNR. Thus, if the same modulation amplitude were used in the laser scan, the 2f signal could only be optimized for one species, while the other one would be either under- (m <2.2) or over-modulated (m > 2.2). To address this problem, we have designed a scan with two different modulation amplitudes at different parts of the scan. An example of a laser scan signal with dual modulation amplitudes is shown in Fig. 5. Such a laser scan signal can be easily generated with a DAQ using its arbitrary waveform output capability. At 20 kHz modulation frequency, a 11-mA modulation depth gives a modulation index m ~2.3 for the ambient N_2O P(22)

#177525 - $15.00 USD Received 5 Oct 2012; revised 21 Nov 2012; accepted 21 Nov 2012; published 3 Dec 2012
(C) 2012 OSA

transition, while a 7-mA modulation depth gives a modulation index *m* ~2.2 for the targeted ambient CO transition. Nitrous oxide is slightly over modulated to make the 2f signal less sensitive to the change of absorption linewidth, which is a function of temperature and pressure. This helps to improve the stability of the measurement under the small changes of environmental conditions. Simultaneous optimization for both absorption lines of N_2O and CO is achieved through the dual modulation amplitudes.

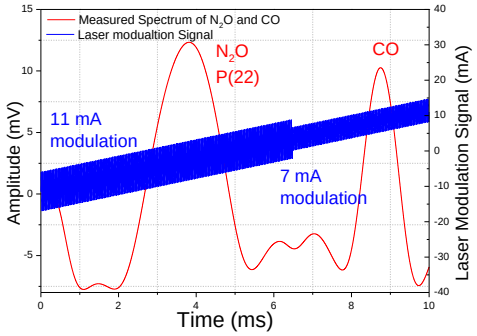

Fig. 5. Dual modulation amplitude laser scan and the corresponding 2f signal.

Another important issue related to probing air-broadened and overlapping absorption features (P(22) N_2O line and nearby CO line) in open-path sensors is spectral interferences. We have performed sensitivity simulations using our numerical model to examine the interferences between the two absorption lines. Figure 6 shows the 2f and 4f spectra of the simulation based on the actual parameters used in the sensor. In the actual atmosphere, the range of atmospheric CO concentrations (~40 ppbv to low ppmv levels) is much larger than those of N_2O (<1%). Thus, the concentration of CO was changed two orders of magnitude in the simulation, while the concentration of N_2O was kept constant. The increase of CO has a slight influence on the N_2O peak in the second harmonic spectra. The 2f peak-to-trough height of the N_2O peak decreases by 2.8% as the CO increases from 0.1 ppm to 15 ppm, while the 4f peak-to-trough height of N_2O only decreases by 0.22%. The interference between two absorption lines is insignificant under most atmospheric conditions and can be minimized by using higher harmonics. Full spectral fitting, which is conducted in our analyses, also helps to further minimize the interference versus using peak-to-trough signal amplitudes.

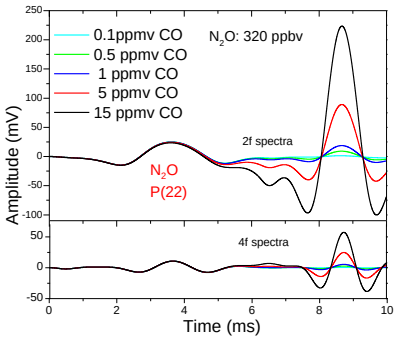

Fig. 6. Calculated spectral inferences between elevated CO and the ambient N_2O signal.

3.3 Calibration with an in-line acetylene reference cell

C_2H_2 is an ideal gas for an in-line reference signal for the N_2O measurement. It has absorption peaks close to the N_2O transitions P(18) and P(23) as shown in Fig. 2. The mole faction of C_2H_2 in the actual environment is less than 1 ppbv in most of the atmosphere with maximum

#177525 - $15.00 USD Received 5 Oct 2012; revised 21 Nov 2012; accepted 21 Nov 2012; published 3 Dec 2012
(C) 2012 OSA

levels of 10 ppbv in highly polluted cities [26]. The low concentration of ambient C_2H_2 coupled with its weak line strength does not influence the measurements of N_2O and CO. The linewidth of C_2H_2 under a reduced pressure in the reference cell is much smaller than that of ambient gas molecules, which also helps to reduce the influence of any possible ambient C_2H_2. Figure 7 shows the experimentally-measured 2f and 4f signals of N_2O/CO with and without the C_2H_2 reference cell for the wavelength region around P(23) N_2O lines under an uniform modulation amplitude. The addition of the C_2H_2 reference cell doesn't influence the 2f/4f spectrum for either N_2O or CO. The WMS detection method easily resolves all three lines within a single laser scan. In order to get a stable C_2H_2 reference signal, a temperature sensor is attached to the reference cell to measure the cell temperature and correct the cell pressure (via ideal gas law) in real time. Simultaneous 2f/4f spectral fitting using the numerical model described previously retrieved the N_2O/CO concentrations from the concentration of C_2H_2 in the reference cell.

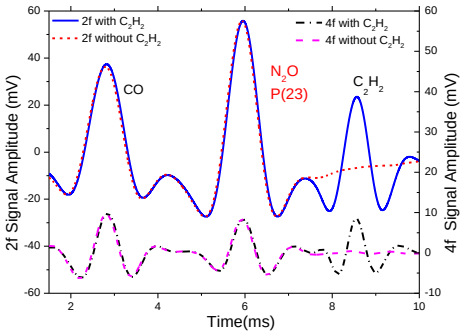

Fig. 7. Comparison of measured N_2O/CO spectra (2f, 4f) at ambient conditions with/without the C_2H_2 reference cell.

3.4 Data retrieval

In WMS, different methods [27] have been used to retrieve the gas concentration from the harmonic signals. A simple way is to measure and calibrate the central peak amplitude (or peak-to-through height) of the 2nd harmonic signal, which is proportional to the gas concentration in an optical thin condition. However, this method only works with well regulated gas temperature and pressure. Another common way is to fit multi-harmonic signals with an analytical expression, which is relatively slow and not suitable for *in situ* analysis due to the complex mathematical calculation. A compromised method is to retrieve gas concentrations based on measured reference spectra [16], which generally requires multiple reference spectra at different atmospheric conditions for open-path detection. Instead of using the above methods, we have developed a real-time multi-harmonic spectral fitting program based on our numerical model. In this LabVIEW-based program, we integrated the software lock-in amplifier with the real-time spectral fitting by using the same IIR filter settings. A least-squares curve fit is then performed to estimate the gas concentration. The fitting spectra are generated through a Voigt line shape with parameters from HITRAN based on the real-time measured air temperature and pressure, which are updated every 2 s. We didn't specifically test the HITRAN parameters. However they should be close to real values, otherwise the fitting or the modulation index should be off. Figure 8 shows an example of the real-time spectral fittings with the residual. In this case, both the 2nd and 4th harmonics were fit simultaneously at 10 Hz. A slight asymmetry in both spectra caused by the intensity modulation [18,19] has been well captured by the fitting curves. The 2nd harmonic signal has larger SNR than the 4th harmonic signal. Thus, the fitting result of the 2nd harmonic signal is used to retrieve gas concentrations. At the same time, the fitting result of 4th harmonic signal is also saved as a reference for data quality control as different harmonics should respond

#177525 - $15.00 USD Received 5 Oct 2012; revised 21 Nov 2012; accepted 21 Nov 2012; published 3 Dec 2012
(C) 2012 OSA

similarly when the concentration changes. The spectral fitting provides a reliable way to retrieve gas concentrations for open path detection under variable atmospheric conditions.

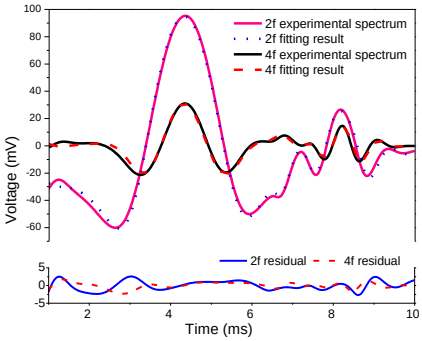

Fig. 8. Real-time spectral fittings for the 2nd and 4th harmonic signals of N_2O and C_2H_2.

4. Results and discussion

4.1 Sensor performance

The sensor was first tested in the laboratory to examine its performance. During this experiment, a tube was placed around the multi-pass cell under ambient, laboratory conditions and partially-sealed the optical cell (aside from the input/exit hole on one mirror). The normalized peak-to-trough amplitudes of the 2f/4f signals were recorded at 20 Hz. The normalization of laser intensity for the 2f signal was performed by using the 1f signal as describe in Rieker *et al* [28]. Figure 9 (a) shows the 20 Hz raw data time series and a histogram of the resulting data. The histogram of N_2O concentrations has an excellent fit to a normal distribution with a HWHM of 0.25 ppbv, which means the major noise during the measurement time was Gaussian (white noise). An Allan deviation analysis [29] was performed and shown in Fig. 9 (b) for both N_2O and CO with a 4-hour long data set. The sensor achieves a precision of 0.15 ppbv of N_2O and 0.36 ppbv of CO with 10 Hz sample rate, equivalent to ~0.1% of the ambient concentrations. The turning point of the Allan deviation curve is approximately 5 s with an optimal sensitivity of ~50 pptv for N_2O. The causes of the observed short term drift are likely due to the environmental temperature and pressure changes, electronic noise and the instability of the optical cell. However, for averaging times as long as 1000 s, the Allen deviation value for N_2O is still smaller than 0.3 ppbv.

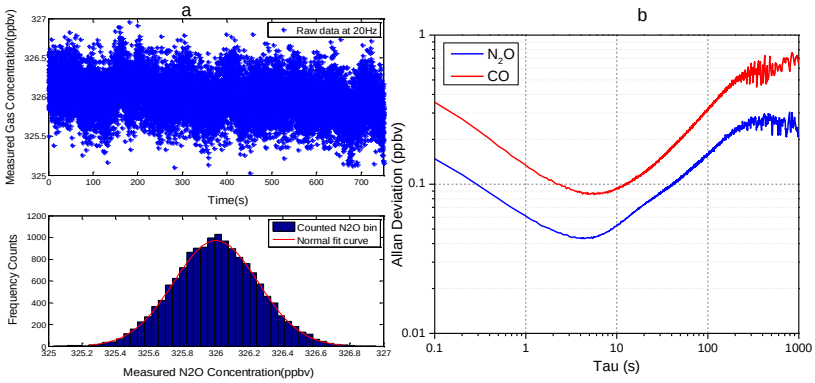

Fig. 9. (a) Example of 20 Hz N_2O raw data and its distribution histogram. (b) Allan deviation plot of N_2O and CO.

#177525 - $15.00 USD Received 5 Oct 2012; revised 21 Nov 2012; accepted 21 Nov 2012; published 3 Dec 2012
(C) 2012 OSA

The performance of the inline calibration cell has also been tested with the sensor placed outside the laboratory, where the ambient conditions are more variable. Figure 10 (a) shows a three-hour experiment with the sensor under a mix of sunshine and clouds. For the ease of visualization, the spectral fitting results for both N_2O and C_2H_2 from the LabVIEW program were averaged to 1 min. Both signals contain lots of variability from the system drift caused by environmental conditions changing (e.g. temperature, sun/shade, and wind). The reference C_2H_2 signal should not change with time after pressure correction due to temperature changes based upon the ideal gas law. Thus, the N_2O signal was calibrated based on the known C_2H_2 reference cell signal and plotted underneath. The addition of inline C_2H_2 reference cell helps to correct the system drift and improve the stability of the sensor. The Allan deviation of the sensor with inline calibration cell was calculated with a 2h long flat section of field measurement as shown in the Fig. 10 (b). The decreasing red line in the graph gives the theoretically expected $1/\sqrt{\tau}$ behavior for a system dominated by white noise. It does show dramatic improvement in terms of stability with a much longer turn-over time of ~400s. The spectrum fitting shows worse precision than the peak-to-trough measurement, a similar result observed and discussed by Hangauer *et al* [27]. Notice the measurement was performed under real field conditions in this case. Parts of the variability may be the real atmospheric changes, and thus this represents an upper limit to the instrument precision. The performance of our sensor is comparable to the results reported in Neftel *et al* [21].

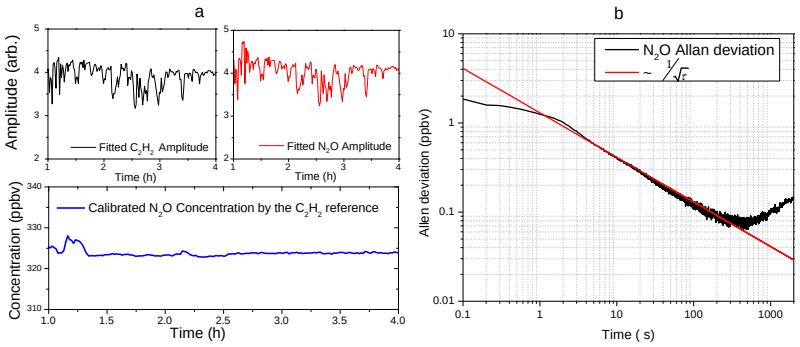

Fig. 10. (a) Field tests of the C_2H_2 inline reference signal and its effect on normalizing the ambient N_2O concentration. (b) Allan deviation plot of field measured N_2O.

4.2 Field Deployment

A field deployment was conducted in Baltimore, MD as part of the Baltimore Ecosystem Study from October 24 to November 2, 2011. The test site was on the campus of the University of Maryland Baltimore County (UMBC), which is a mixed use area with forest, suburban lawns and nearby freeways. An automatic weather station (Vaisala WXT520) was setup beside the sensor to provide meteorological measurements including temperature, pressure, relative humidity and rainfall rate, etc. The sensor operated continuously during the deployment, while the values of different setting parameters were adjusted to test the performance of the sensor under various operation conditions. The concentrations of N_2O and CO were captured at 10 Hz, while the 2f/4f spectra and direct absorption spectra were saved every hour for calibration. During the post processing, the measured temperature and pressure from the weather station were used as the input parameters for the spectral fitting, while relative humidity was used as a dilution factor to correct the concentrations. Figure 11 (a) shows a strong increase of the measured N_2O concentration with the rainfall rate during a rainy day during the deployment, while the CO concentration had no significant correlation. The ambient N_2O concentration increased with the rainfall rate, which suggests that more N_2O was emitted from the soil, one of the largest natural sources of N_2O. Both the nitrification and denitrification processes occurring in the soil can generate N_2O emissions.

#177525 - $15.00 USD Received 5 Oct 2012; revised 21 Nov 2012; accepted 21 Nov 2012; published 3 Dec 2012
(C) 2012 OSA

Such increases of N_2O during precipitation have been observed by other researchers [21,30,31]. The distinct CO diurnal cycles for an urban area were observed as shown Fig. 11 (b) with the data averaged every five minutes. The strong influence from the traffic of the Baltimore area contributed to the increase of the CO concentration during the rush hours. At the same time, the change of the boundary layer height from night to day changed the degree of mixing process and led to a lower CO concentration during the noon time than before dawn.

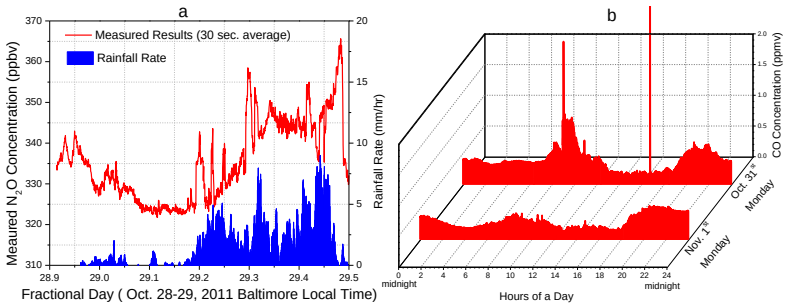

Fig. 11. (a) Measured N_2O concentration during precipitation. (b) diurnal cycle of CO concentration.

At around local time 16:45 (UTC time 20:45) of Oct. 31st, there was a very strong peak in the CO concentration. Figure 12 (a) is a time series of that particular event with both the N_2O and CO concentrations shown at 10 Hz. The increase of CO was coincident with the increase of N_2O. The CO mixing ratio reached as high as ~18 ppm, which introduced both a nonlinear response in 2f concentration and also the interference to N_2O as discussed previously. Thus, post correction was performed with the model simulation to retrieve the actual concentrations from the interference and saturation effects. Figure 12 (b) is a correlation plot between corrected N_2O and CO concentrations in the peak region. The N_2O and CO concentrations show a positive linear correlation with R^2 ~0.987. This indicates that there was a strong anthropogenic N_2O source nearby as CO emissions largely come from anthropogenic activities like combustion. In this case, it likely was the emission of a nearby vehicle. The mass emission of N_2O/CO can be roughly estimated through multiplying the molecular weight with the integration of the area for each overshoot beyond the baseline. The calculated mass emission ratio of N_2O/CO for this event is around 1/275 g/g, which is consistent with motor vehicle emissions from the EPA [32, 33].

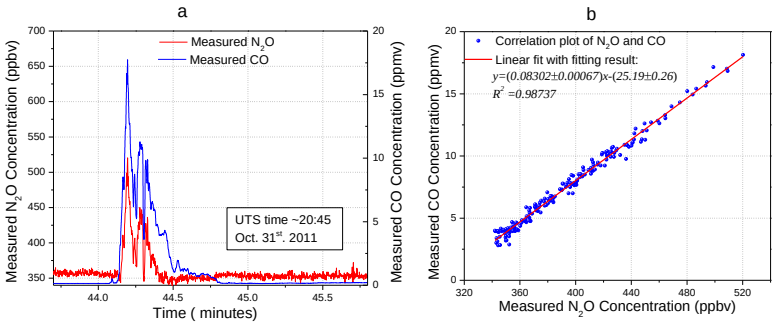

Fig. 12. (a) Peaks of N_2O and CO. (b) correlation for the increase of CO/N_2O concentrations.

4.3 Influence of Water Vapor

One of the most important impact factors for atmospheric gas sensing is the effect of water vapor. Neftel *et al.* [16] have shown the importance and difficulty of performing water vapor

#177525 - $15.00 USD Received 5 Oct 2012; revised 21 Nov 2012; accepted 21 Nov 2012; published 3 Dec 2012
(C) 2012 OSA

corrections in N_2O flux measurements. Water vapor not only has the dilution effect but also can influence the absorption linewidth [34]. Hence, a comprehensive study is needed to calibrate the spectroscopic influence of water vapor to the target absorption lines, which then can be used as correction factors for open-path detection. Here, we perform a model simulation to roughly estimate the magnitude of influence for neglecting water vapor broadening effect to the measurement.

The parameters of the P(23) N_2O line were used in the simulation with its air-broadening linewidth of 0.0734 cm^{-1}/atm and self-broadening linewidth of 0.0940 cm^{-1}/atm. Based upon these values, the water vapor broadening linewidth was estimated from 0.05 to 0.15 cm^{-1}/atm. For a 0-3% change in absolute H_2O concentration, the N_2O linewidth changed to ~99% (0.05 cm^{-1}/atm) and 103% (0.15 cm^{-1}/atm) of the value without water vapor. The simulated results show that if the N_2O linewidth is changed by 1% due to the water vapor pressure broadening influence, the measured gas concentration is also changed by 1% from fitting of the 2nd harmonic spectra. Similar as the experimental result from Neftel *et al* [16], the change in measured gas concentration proportionally increases with the mole fraction of water vapor. During above field results, measurements of the local dew point varied between 1.5 and 3.2°C measured by the Vaisala WXT520, corresponding to a mole fraction range of water vapor of 0.68-0.78%. Based upon the highest sensitivity above (0.15 cm^{-1}/atm), neglecting the observed variations in H_2O results in an uncertainty of N_2O mole fractions of ~0.1%, which is much less than the observed variability of N_2O. Thus, the influence of water vapor broadening effect was not significant at these conditions but certainly would be important for higher variability of absolute humidity.

5. Conclusion

We have shown the development of a compact, low-power and field-deployable QCL-based N_2O/CO sensor with WMS in an open-path configuration. An inline C_2H_2 reference cell is demonstrated as a simple and convenient way for calibration and minimizing system drift for long-term observations and rapidly-changing conditions for open-path configuration. We introduced a new numerical WMS model based on direct simulation of the detector signal through the lock-in amplifier. Along with the model, a LabVIEW-based software lock-in amplifier is also developed and integrated in the sensor to achieve fast multi-harmonic detection. A special laser modulation scheme with dual modulation amplitude is used to optimize the detection of both N_2O and CO. Measurements of the sensor from a recent field deployment are presented in this paper to evaluate its preliminary performance. The simultaneous detection of N_2O as well as CO offers new insight into exploring the various sources for N_2O emissions. We observed the biogenic N_2O emissions from the soil during precipitation as well as anthropogenic N_2O emissions from motor vehicles. Distinguishing between these two sources by the simultaneous CO measurements shows the usefulness of the proposed sensor. The present study provides a clear pathway for precise and stable N_2O measurements from open-path sensors in remote field environments.

Acknowledgments

This work was supported by NSF grant EEC-0540832, USDA Air Quality (2008-35112-05274), Center for Mid-Infrared Technologies for Health and the Environment (MIRTHE) and an anonymous private donor. The authors acknowledge the groups of Profs. Gerard Wysocki, James Smith and Elie Bou-Zeid for providing helpful discussions and loaning of equipment.

#177525 - $15.00 USD Received 5 Oct 2012; revised 21 Nov 2012; accepted 21 Nov 2012; published 3 Dec 2012
(C) 2012 OSA